Wind induced vibrations on large observation wheels

Giorgio Diana[1], Tommaso Argentini[1], Mirsad Barucic[2], Marco Belloli[1],
Stefano Giappino[1], Marc Groenendijk[2], Sara Muggiasca[1]
[1]Politecnico di Milano, Department of Mechanical Engineering, Italy
[2]KCI the engineers B.V., The Netherlands
email: stefano.giappino@polimi.it

ABSTRACT: Modern observation wheels are extremely high, slender and light structures, making them particularly sensitive to the wind actions. In the design stage aerodynamics is one of the issues to be investigated since the structure may experience wind-induced vibrations. The paper reviews the phenomena related to wind-structure interaction. The aerodynamic design of a new observation wheel is than presented.

KEY WORDS: Wind Induced Vibrations; Observation Wheel; Cables Aerodynamics; Wind Tunnel Tests.

1   INTRODUCTION

The first modern observation wheel was built for the Chicago world fair of 1893 by George Ferris. The structure was 80.4 m high and hosted 36 passenger cars, each with a capacity of 60 people, giving a total capacity of 2160. Since that period a relevant number of observation wheels has been built so far, often with the aim to break the previous height record.

Significant structures to be mentioned are the British Airways London Eye (*135m*), built for the millennium celebrations and the highest in Europe, the Singapore Flyer (*165m*) and the Las Vegas High Roller (*167.5m*) that is the current world tallest as summarized in Table 1. Relevant projects are planned or under construction like the New York High Wheel (*192m*) and the Dubai I (*210m*). These structures are often extreme engineering challenges, due by their size but also by the shape layout asked by architects to improve their beauty. In Figure 1 a sketch of an observation wheel shows the main components: the wheel is a circular structure composed by the rim and the capsules that host passengers and the hub. Tensioned cables are used to connect the rim to the hub. The hub is supported by a columns structure that is named A-frame due to its shape like an A.

N.	Name	High [m]	Year	City	Country
1	High Roller	167,6	2013	Las Vegas	USA
2	Singapore Flyer	165	2008	Singapore	Singapore
3	Star of Nanchang	160	2006	Nanchang	China
4	London Eye	135	1999	London	United Kingdom
5	The Southern Star	120	2008	Melbourne	Australia
6	Changsha Ferris Wheel	120	2004	Changsha	China
7	Zhengzhou Ferris Wheel	120	2003	Zhengzhou	China
8	Sky Dream Fukuoka	120	2002	Fukuoka	Japan
9	Diamonds and Flowers	117	2001	Tokyo	Japan
10	Sky Wheel of Odaiba	115	1999	Odaiba	Japan

Table 1 World's 10 largest Observation Wheels

1 Capsule
2 Rim
3 Spoke Cables
4 Spindle & Hub
5 A-frame Columns
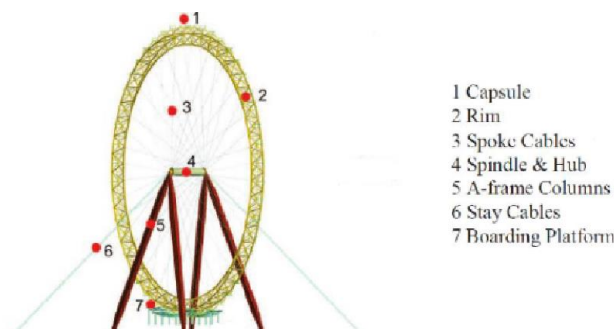6 Stay Cables
7 Boarding Platform

Figure 1 Main parts of an observation wheel according to Zhao and Ding, (2010)

Large observation wheels have generally small peripheral speed in the order of 1 km/h that corresponds to about 30 minutes per turn.

2 OBSERVATION WHEELS AERODYNAMICS

The wind is one of the most crucial factors affecting the design since all the effects of the interaction between wind and structure have to be taken into account: vortex shedding and vortex induced vibrations, wake induced vibrations and galloping. Different flow induced vibration phenomena may be experienced by these components and will be investigated separately on the spoke cables and on the A-Frame. The rib can experience a significant drag force, depending on the shape of the capsules (Allsop et al., 2009) but generally gives an aerodynamic damping contribution to the structure and it is not subjected to flow induced vibrations.

2.1 Spoke cables

Tensioned cables are used to connect the rim to the spindle, like in a bicycle wheel, and they give lightness to the structure. The arrangement of the spoke cables provides the stiffness to the rib and influences the response of the wheel to lateral wind (Allsop et al., 2009). Cables are structures very sensitive to the wind actions and they may suffer from different kinds of flow-structure interaction: vortex shedding and galloping, typical problems observed on the stays of a cable-stayed bridge i.e. flexible cylinder characterized by low frequency and small structural damping often inclined with respect to the wind. Vortex shedding on circular cylinder is a well known phenomenon when the cylinder is perpendicular to the flow, few studies are available for inclined cables. In particular some researchers (Hogan and Hall, 2010; Jain, 2012) found that if the inclination angle between the wind and the cable axis is not far from 90°, the phenomenon is still present but related to the wind speed component perpendicular to the cylinder axis, otherwise the inclination may disorganize the flow around the cylinder suppressing periodic vortex shedding. This can be explained considering the axial flow that appears when the inclination angle become relevant: the axial flow disturbs vortex shedding avoiding synchronization. Due to the importance of the tridimensionality of the flow around the cylinder in vortex shedding definition, also the boundary conditions can be considered essential, both in the real case and in the wind tunnel tests. Also the cable surface plays an important role interfering with the vortex detachment but also with the axial flow (Matsumoto, 1998; Matsumoto et al., 2010). In particular surface roughness or devices applied on the surface can reduce oscillation amplitudes induced by vortex shedding, but they can also reduce the disturb effect of the axial flow.

Vortex shedding vibrations for the spoke cables of an observation wheel generally concerns low wind velocities and structural frequencies higher than 2 Hz. The natural frequencies change when the wheel is revolving because of the different contribution of gravity force as a functions of the spoke position. For this reason vortex shedding is more critical for the structure when the wheel is still and the frequencies do not change.

At higher wind velocities other aerodynamic phenomena may occur as ice-galloping, rain-wind induced vibration, high-speed vortex excitation and dry inclined cable galloping.

Ice-galloping and rain-wind induced vibration are low frequency, large amplitude instability phenomena related to asymmetries on the cable section due to ice formation or rain rivulet respectively. These asymmetries generate lift force on the cable and if the slope of the lift force as a function of the ice/rivulet angular position is negative this can be indicative of a possible instability. This condition become more critical if it turns out at the same time of the drag crisis.

Dry inclined cable galloping is a divergent type of motion that may happen with no precipitations when a cable is not perpendicular to the wind: the inclination compromises the geometrical symmetry of the cable with respect to the wind creating a tridimensional flow, source of the galloping instability. This phenomenon can be considered as a mechanism similar to that of the classical galloping. Few studies highlighted this phenomenon on smooth inclined cables: Honda et al. (1995), Miyata et al. (1994) Saito et al. (1994), Cheng et al. (2003).

High-speed vortex excitation is a limited amplitude cable motion that looks more like vortex shedding rather than galloping. Large amplitudes occurred in a limited wind velocity range as observed by Matsumoto (1998), Jakobsen et al. (2012), Cheng et al. (2003).

In Cheng et al. (2008) both dry inclined cable galloping and high speed vortex excitation were studied. It is pointed out that in case of dry galloping the divergent motion happened when drag force decreases and the lift coefficient curve has a negative slope. On the other hand neither drag crisis nor negative lift slope were observed in case of high-speed vortex excitation. Matsumoto (1998) suggested that this mechanism can be considered affected by the coupling between vortex shedding in the wake and along the cable axis.

The comparison made in Cheng et al. (2008) with the results obtained in previous studies (Honda et al. 1995; Miyata et al. 1994; Saito et al. 1994) highlights that in similar conditions different galloping response can be found: that evidence points out that galloping phenomena are very sensitive to many factors and it is not easy to identify guidelines to predict inclined cable response.

Even if the occurrence of these phenomena is not well known, otherwise in order to avoid undesirable vibrations, appropriate damping systems have to be designed. In order to define the characteristic required for the damping system, the cable response can be predicted also using some numerical model. For the aeolian vibrations, for example, the cable behavior can be simulated using a model based on an energy balance between the energy input from the wind and the one dissipated by cable and damping devices (Energy Balance Principle). This model, generally used for overhead transmission line, can be easily applied also to other kind of cables (Diana, 2000). For a more detailed modeling of the flow-structure interaction when vortex shedding occurs, there are some time domain models able to reproduce the non linear aerodynamic forces acting on a cable in lock-in region (Hartlem

and Currie, 1970; Manenti et al. 2007). These models can be adapted to different interaction conditions but require preliminary experimental tests in order to correctly estimate the parameters for the forces definitions.

Also for the galloping instability as ice-galloping it is possible to use numerical models to predict the dynamic response of the cable. In particular the studied cable can be reproduced through finite element model, while the aeroelastic forces can be modelled using the static coefficients obtained from literature or experimentally, and the quasi-steady theory (see Diana, 2000).

The aerodynamic forces when galloping instability occurs change slowly with respect to cables frequency differently to what happen in vortex shedding conditions. For this reason these forces can be defined using the quasi-steady theory knowing the static coefficients as a function of the angles of attack of the wind. The so defined forces can be introduced in the motion equations of the structure. If it is not required to define the cable response but just a stability criterion is needed to point out if the structure can show a critical behavior, the following condition, developed by Den Hartog (1932), identifies the condition of possible instability based on quasi-steady theory:

$$\left(\frac{\partial C_L}{\partial \alpha} + C_D\right)\Big|_{\alpha=\hat{\alpha}} < 0$$

The criterion suggests that the instability may occur when the lift coefficient has a negative slope and the drag coefficient reaches low values. Macdonald and Larose, (2006) developed a more complex formulation that takes into account the dependence of the instability on some other parameters: in particular they introduce the dependence on Reynolds number and on all the angles that define the position of a cable with respect to the wind direction. Models that take into account two degrees of freedom have also been developed (Luongo and Piccardo, 2005; Carassale et al., 2005).

Vortex induced vibrations are generally the most important problem to deal with and an efficient strategy to control the vibrations must be defined. Modification of the surface layout, like the helical fillet can reduce vortex induce vibrations and it may disturb galloping instability, but this reduction could not to be enough for the structure safety. To control the vibration of modes higher that 2 Hz Stockbridge type dampers can be used because they work for a frequency range between 2 up to 20-40 Hz. These devices can control vortex induced vibrations because, even if the system is characterized by frequencies lower than 2 Hz, the phenomenon is not able to introduce enough energy in the system for too low frequencies. The amount of damping needed to control VIV is generally adequate to control also the other flow-induced phenomena. An exception are the very low frequencies of the system that are not excited by vortex shedding but can be subjected to galloping instability. A special type of TMD able to control frequencies lower than 2 Hz or, otherwise, other kind of dampers, for example hydraulic damper as in (Cigada et al., 2000) can be used.

2.2   *Supporting structure*

The supporting structure is the part that has to support the rotating wheel. Its height is related to the diameter of the wheel and often exceeds 100 meters. Typically it is realized by 2 or more columns having a circular section (London Eye, Singapore Flyer, Dubay I). These are slender, light and low damped structures, making them sensitive to wind effects. The columns may experience vortex shedding and mitigation devices like tuned mass dampers have to be installed like in the Singapore Flyer (Allsop et al., 2009). In case of close columns interference is possible and instability phenomena like wake induced vibrations have to be investigated. For extremely light structures we should also consider the buffeting response.

In many cases cable stays are used to stabilize the supporting structures. Cable stays wind induced problems are similar to the spoke cables ones previously described (Diana et al., 2000).

A particular layout is the London Eye, where the columns are only on one wheel side and the wheel overhang the Thames River.

3   TEST CASE: A NEW OBSERVATION WHEEL

The aerodynamic design of a new observation wheel is hereafter described, showing the possible sources of flow induced vibrations and mitigation procedure. The observation wheel is 210m height and has a total weight of about 10100 ton. It was decided to perform different ad hoc wind tunnel experiments on the supporting frame on a scaled model and on the spoke cables on a 1:1 prototype cable.

3.1   *Spoke cables*

The static and dynamic behavior of the rim spoke cables was studied by means of wind tunnel tests on cable prototypes. Two different layouts of the spoke cables were considered: type I cable (Figure 2a), covered with a HDPE tube and a helical strake and type II cable characterized by the presence of led and power cables to feed spoke led lights (Figure 2b). The helical fillet has two principles, a semicircular section 2 mm protruding from the surface, a helix angle of 70.4° and a pitch of 420 mm. All the tests were performed in the Politecnico di Milano wind tunnel high speed test section as showed in Figure 2a. The main characteristics of the tested models are reported in Table 2.

		roped	led
length	*m*	3.5	
external diameter D	*mm*	95	
linear mass	*kg/m*	5.16	5.84

Table 2 Main data of the wind tunnel models
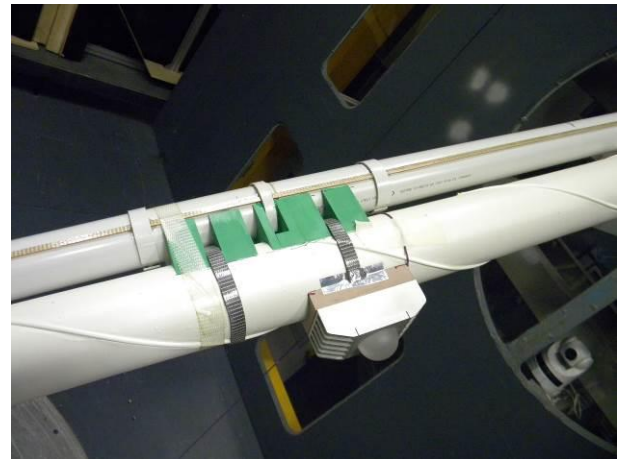
(a) type I "roped" (b) type II "led"

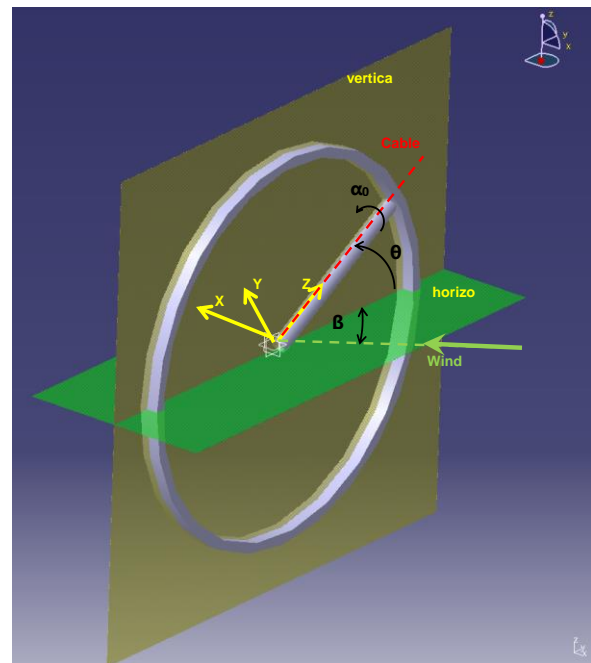Figure 2. Wind tunnel spoke models: (a) roped layout and (b) led layout.

3.1.1   Model set-up

Both the models were tested using the same arrangement in the wind tunnel test section: this particular set up allowed to carry out static and dynamic tests. The spoke model is constrained at the low end to the ground, while the top end is free, reproducing a cantilever beam. In order to avoid sharp edges on the top, the free end is fitted with a semispherical plug. A force balance is placed between the model and the floor in order to measure aerodynamic forces. The model is connected to the balances through a steel plate and an axle flange. The flange is glued to the cable and has a free threated shaft. The shaft is connected to the plate allowing this joint the rotation with respect to the cable axis (α_0). Below the two balances a second steel plate is placed, this plate is connected to the ground (wind tunnel turntable) through a hinge that allows the inclination of the cable (θ angle). A connection rod allows to fix the cable at the desired inclination. The rotation of the cable with respect to the wind (β angle) is allowed by the wind tunnel turntable.

The three rotation angles are sketched in Figure 3(a). In Figure 3(b) the rotation angles are showed in relation to the position of the spoke in the wheel.
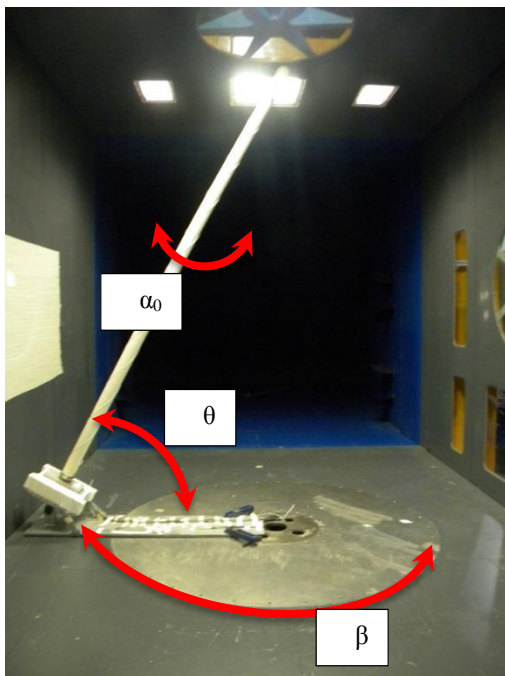
(a) Rotation angles in the wind tunnel test section (b) Rotation angles with respect to the observation wheel

Figure 3. Cable rotation angles

An alternative couple of angles can be introduced to define the aerodynamic forces from a different point of view: angles ϕ and α_U. These angles can be useful especial to study the second configuration (type II 'led') and they can related to the previous ones through the equations:

$$cos(\phi) = cos(\beta)cos(\theta)$$
$$tan(\alpha_U) = \frac{sin(\theta)}{tan(\beta)}$$

Figure 4 and Table 3 better clarify all the used angles.

Angle	Name	Description
θ	cable angle	The vertical angle between the cylinder axis and the horizontal direction
β	wind angle	Angle of the incoming wind direction in the horizontal plane
α_0	LED angle	LED orientation angle
ϕ	cable-wind angle	Relative angle between the wind direction and the cable axis
α_U	X-wind angle	Angle between the normal component of the wind velocity and the X local axis

Table 3 Main cable angles

The sum between α_0 and α_U gives the absolute angle α_{ass}.

$$\alpha_{ass} = \alpha_0 + \alpha_U$$
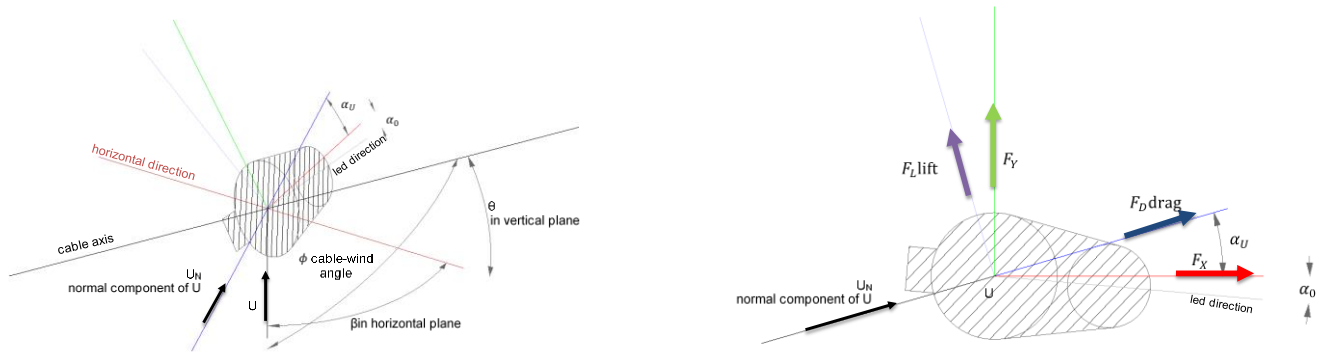
Figure 4 Main angles and reference direction

The aerodynamic forces were considered in terms of non-dimensional coefficients both in the X-Y reference system and in the drag-lift system (see Figure 3 and Figure 4). The coefficients are defined as:

$$C_{Fx} = \frac{F_X}{\frac{1}{2}\rho U^2 DL} \qquad C_{Fy} = \frac{F_Y}{\frac{1}{2}\rho U^2 DL}$$
$$C_D = \frac{F_D}{\frac{1}{2}\rho U^2 DL} \qquad C_L = \frac{F_L}{\frac{1}{2}\rho U^2 DL}$$

The same coefficients can be also calculated using an alternative normalization: only the wind velocity component normal to the cylinder axis ($U_N = U \sin\phi$) is considered. This kind of normalization is often used in literature to highlight the contribution due to the wind that acts perpendicular to the cable.

The aerodynamic coefficients were calculated during static tests where the models are tested at different inclinations angles and different wind velocities up to 50 m/s for roped cable and up to 30 m/s for led cable.

During dynamic tests the behavior of the models was investigated by means of two accelerometers placed in correspondence of the free end of the cable, along X and Y directions. During these tests the structural damping was modified using a specific actively controlled device able to reduce the damping of the system: this device analyze the cable acceleration introducing in the system a force opposite to its velocity. Three levels of structural damping were considered.

3.1.2   Results – type I 'roped'

3.1.2.1   Static tests

The static tests were performed for the combination of angles reported in Table 4.

Figure 5(a) and Figure 5(b) show the aerodynamic force coefficient as a function of the wind speed U in the frame of reference X-Y. Figure 5(c) and Figure 5(d) show the drag and lift force coefficients. Drag figure has a second horizontal axis showing the corresponding Reynolds number value calculated on the cable diameter.

When the wind is perpendicular to the wheel plane, that is β=90° (regardless of θ), the drag correspond to the X force and the lift to Y force. In this exposure it is possible to observe that drag starts at a value of about 1.2 and it drops to 0.8 increasing the wind velocity: this is because the cylinder is entering in the critical Reynolds number region. The obtained values are higher with respect to the ones relative to a smooth cylinder: this can be explained considering the effects of the helical fillet that acts like surface roughness modifying the drag curves in their critical region. On the contrary lift has low values: this is also expected since an ideal cylinder, due to his axial symmetry, should have always 0 lift. Non-zero lift values in the experiments can be found due to "imperfection" on the model surface that generates asymmetries in the pressure distribution and so a lift force.

What it is to note is that if we consider the forces in X-Y frame we can observe force coefficients value in Y direction as high as 1. This is due to the combination of wind and cables angles.

Considering drag and lift coefficients normalized on the normal component of wind velocity U_N (Figure 5(e) and Figure 5(f)), it is possible to note that all the drag curves become very similar and also the curve related to the configuration β=30° - θ=30° shows values similar to other curves.

Figure 6 shows the drag and lift coefficients normalized on the wind velocity component normal to the cylinder axis: the coefficients are plotted as a function of the Reynolds Number and the angle ϕ in order to highlight the dependence on both the parameters. In theory, due to the ideal symmetry of a cylinder, the only angle ϕ could be sufficient to define the cable position. Nevertheless the local surface imperfections and the helical fillet affect the cable aerodynamic, possibly giving different coefficients when the angle ϕ is the same while the angle α differs. In this case, the configurations with same ϕ and different α have slightly different coefficients: this highlights how many factors can influence cable aerodynamics.

Considering the slope of the coefficients curves as a function of the angles it is possible to apply the criterion for the galloping instability. The performed tests are just a limited database but they can give an idea about the instability problem. It is important to point out that the higher values measured for the drag coefficients due to the presence of the helical fillet work for the cable stability. On the other hand, further analysis were performed during dynamic tests to check cable stability.

| θ	β	ϕ	α	wind speed
[deg]	[deg]	[deg]	[deg]	[m/s]
30	90	90.0	0.0	10, 20, 30, 40, 50
30	60	64.3	16.1	10, 20, 30, 40, 50
30	30	41.4	40.9	10, 20, 30, 40, 50
60	90	90.0	0.0	10, 20, 30, 40, 50
60	60	75.5	26.6	10, 20, 30, 40, 50
60	30	64.3	56.3	10, 20, 30, 40, 50

Table 4 Static tests on roped cable

3.1.2.2   Dynamic tests

The design set-up grants small oscillation amplitude unless dynamic phenomena occur. Particular attention it was given to vortex shedding and in order to enhance this phenomenon very small value of structural non-dimensional damping was realized (see Table 5). Due to the low value of linear mass, the obtained Scruton number reached small levels, comparable with the real ones.

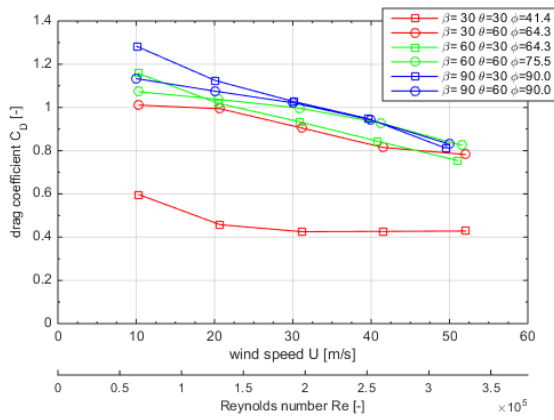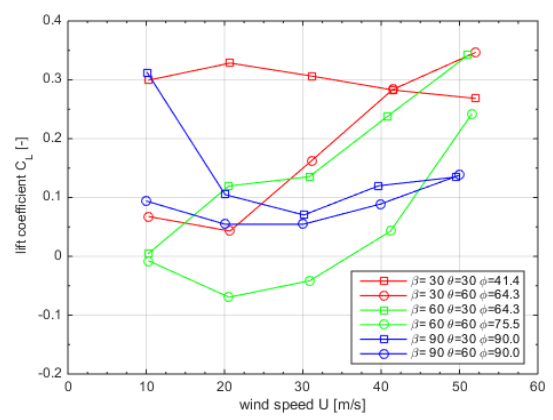|	ζ_s (small amp.)	Sc
	[-]	[-]
r0	1.90E-03	5.8
r1	5.00E-04	1.5
r2	1.00E-04	0.3

Table 5. Structural damping levels
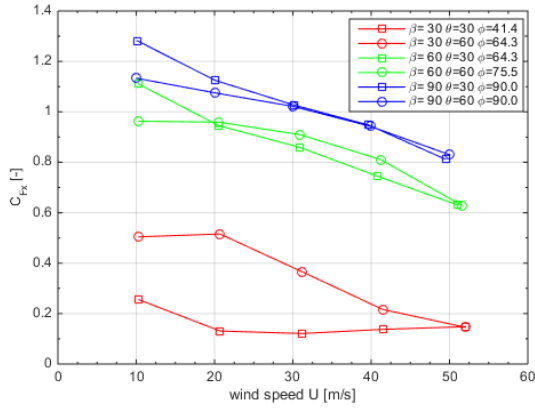
(a) Force coefficient in X direction for different β and θ angles
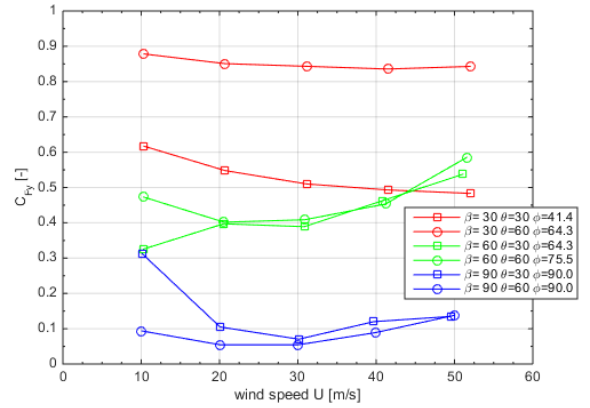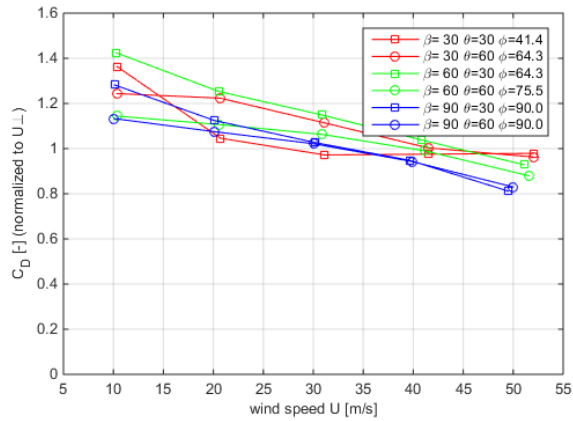
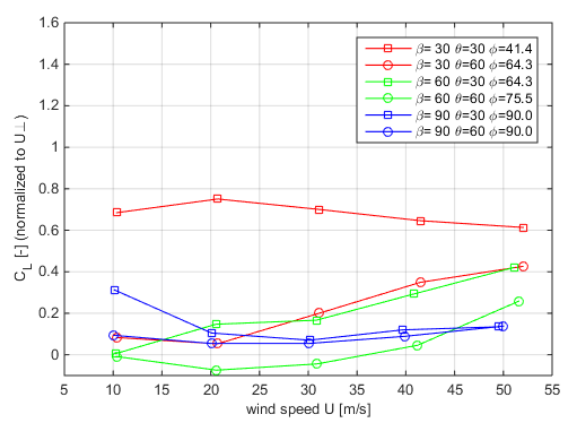(b) Force coefficient in Y direction for different β and θ angles

(c) Drag force coefficient for different β and θ angles

(d) Lift force coefficient for different β and θ angles

(e) Drag force coefficient for different β and θ angles. The coefficient is normalized on the wind velocity component U_N

(f) Lift force coefficient for different β and θ angles. The coefficient is normalized on the wind velocity component U_N
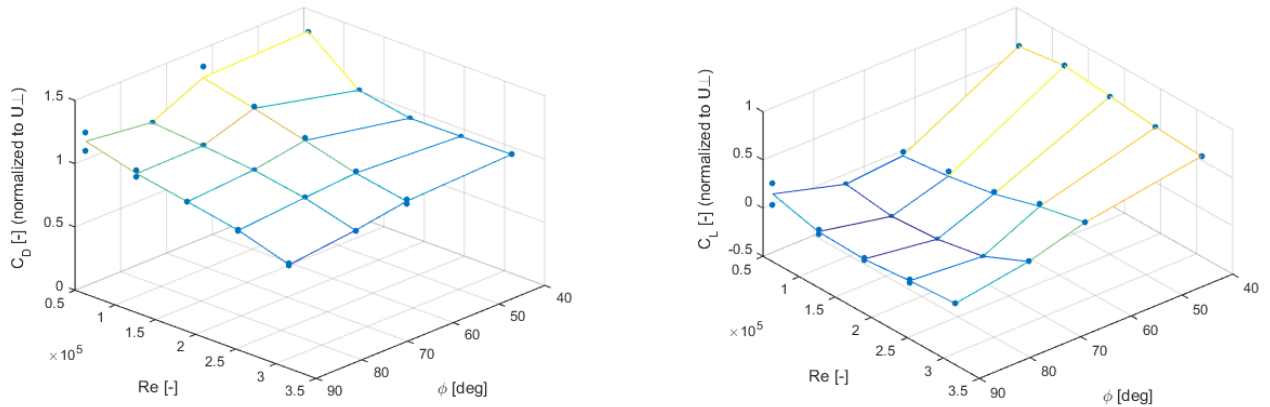
Figure 5. Force coefficients

Figure 6. Force coefficients surfaces

The dynamic behavior of the roped cable was studied for a limited combination of angles reported in Table 6.

θ	β	φ	α	ζ_s
[deg]	[deg]	[deg]	[deg]	[-]
30	90	90.0	0.0	r0,r1,r2
30	60	64.3	16.1	r0,r1
30	30	41.4	40.9	r0,r1
30	-60	64.3	-16.1	r1

Table 6 Dynamic tests on roped cable

In Figure 7 are reported the steady state responses of the cable in cross-wind direction, in particular Figure 7(a) shows the behavior of the model perpendicular to the wind (β=90° and θ=30°) for different level of structural damping and Figure 7(b) shows the behavior of the model for the same level of structural damping (r1) and different values of β. The dynamic response was obtained exciting the first flexible mode of the model in the cross-wind direction (f_N = 3.5 Hz) changing by small step the wind velocity. The data are reported as a function of the velocity ratio calculated as the ratio between current wind velocity and Strouhal velocity (U_S= f_N D/St=1.66 where the Strouhal Number St was evaluated equal to 0.2).

It is possible to note that a reduction of non-dimensional structural damping increases the maximum amplitude reached in the lock-in region and pushes the synchronization region toward higher velocity ratios. The maximum amplitudes reached are consistent with the expected ones for roped cylinders: about a third of the values observed for smooth cylinders.

Figure 7(b) highlights the effects of the inclinations angles on the steady state response for the configuration r1. It is possible to note that inclined cable can experience higher oscillation amplitudes than the configuration perpendicular to the wind direction (β=90°). Matsumoto (2010) highlights that the inclined cable generally experiences lower oscillation amplitudes than the one perpendicular to the wind when its surface is smooth because of the axial flow that interferes with vortex shedding phenomenon, however the helical fillet presence can disturb axial flow resulting in oscillation amplitude higher than expected.
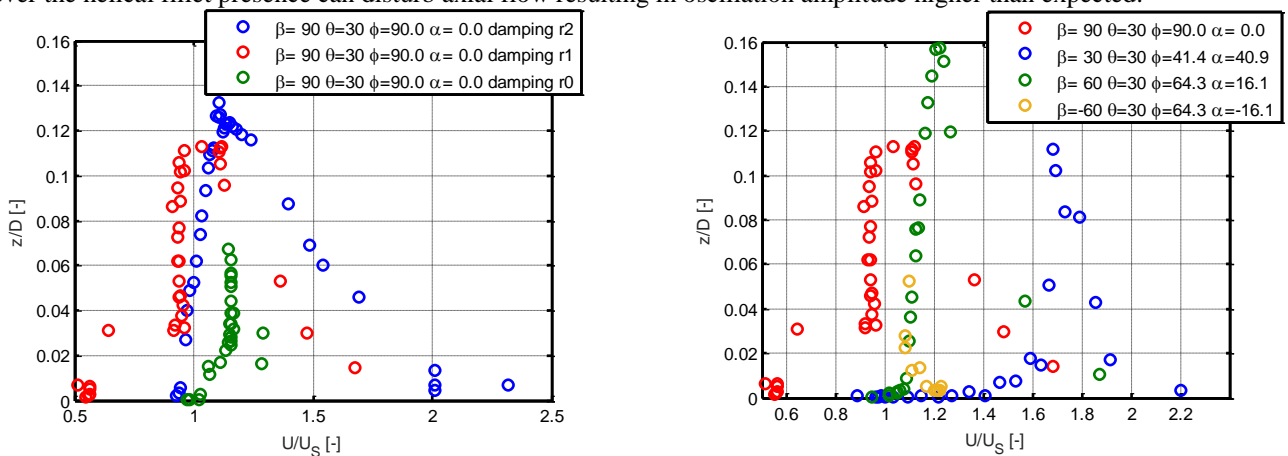

(a) Steady state response for the configuration β=90° and θ=30° for different levels of structural damping

(b) Steady state response for the structural damping r1 for different values of β

Figure 7 Steady state response

The lock-in region can also move toward different velocity ratio ranges, in particular this can be observed for the configuration β=30° - θ=30°. Moreover, comparing configuration β=60° - θ=30° with configuration β=-60° - θ=30° it is possible to note that symmetrical configurations can experience very different level of oscillation amplitude: this can be explained considering that, however the relative angles between wind and cylinder axis are the same, the helical fillet placed on the cylinder surface expose a different profile to the wind. Also small differences on the cable surface can influence vortex shedding response of the model.

Figure 8 shows the specific power input calculated for the tested configurations. Each curve plotted represents the envelope of all the curves obtained for the build-ups performed within the lock-in region. For further details concerning the calculation of the power imparted by the wind when vortex shedding occurs see Diana & Falco (1971), Diana et al. (2005) and EPRI 2006. All the configurations give similar results, consistent with the ones obtained with flexible models. As stated in Diana (2003) flexible models experience lower specific power input than rigid models because the sections along the cables are characterized by different flow-structure interaction.
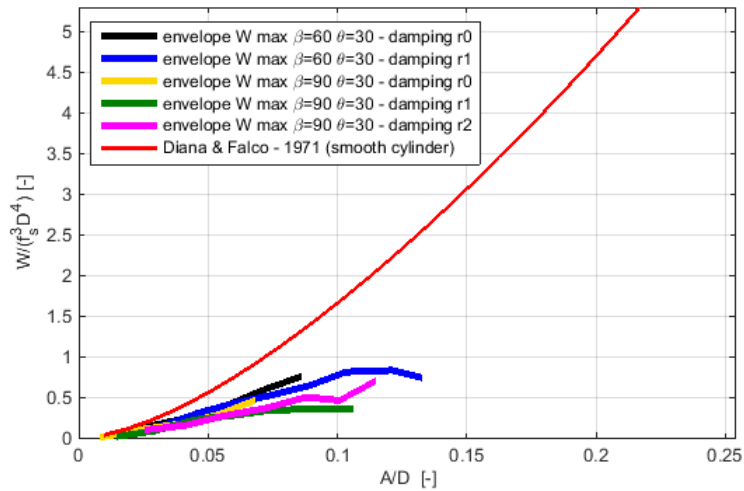

Figure 8 – Maximum power input envelopes for different cable orientation angles

Out of the lock-in region the oscillation amplitudes are quite small and no galloping instability was observed neither dry inclined cable galloping nor high-speed vortex excitation.

3.1.3   Results – type II 'led'

3.1.3.1   Static tests

The led configuration is characterized by a strong modification with respect to the roped cable. In fact, the presence of the led and the led cable (for power supply) has non-negligible effects on the body aerodynamics.
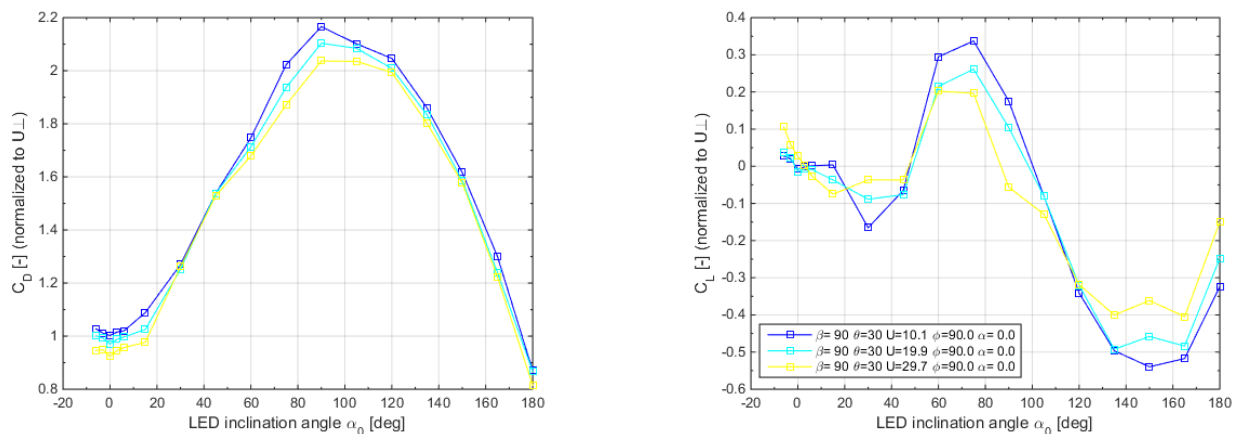
(a) Drag force coefficient for different α_0 angle and for θ=30° and β=90°. The three curves were obtained for different wind velocity

(b) Lift force coefficient for different α_0 angle and for θ=30° and β=90°. The three curves were obtained for different wind velocity

Figure 9 Force coefficients

Figure 9 shows the drag and lift coefficient of the spoke cable in LED configuration as a function of the led orientation angle α_0 when the wind is perpendicular to the cable (β=90°) and θ is equal to 30°. In this exposure drag corresponds to X direction and lift to Y direction. We observe that drag starts at values lower than 1 (0.95) for angles close to 0 and reaches a maximum of 2.04 when wind α_0=90°.

Comparing the curves obtained at different velocities, no significant differences can be observed. Due to the shape of the section, that is strongly modified by the presence of the led cable, we have a variation of the lift force with the led inclination angle. Negative lift derivatives are indication of possible galloping instability.

In order to better investigate possible instability, tests for different combinations of wind and cable angles were performed.

Figure 10 summarize some coefficients measured during the tests for the wind velocity U=30 m/s and as a function of α_{ass} and ϕ. The shape of the aerodynamic coefficients observed for different combinations of cables angles confirm that the spoke cable in led configuration may suffer from galloping instability phenomena.

(a) Drag force coefficient for U=30 m/s and as function of α_{ass} and ϕ

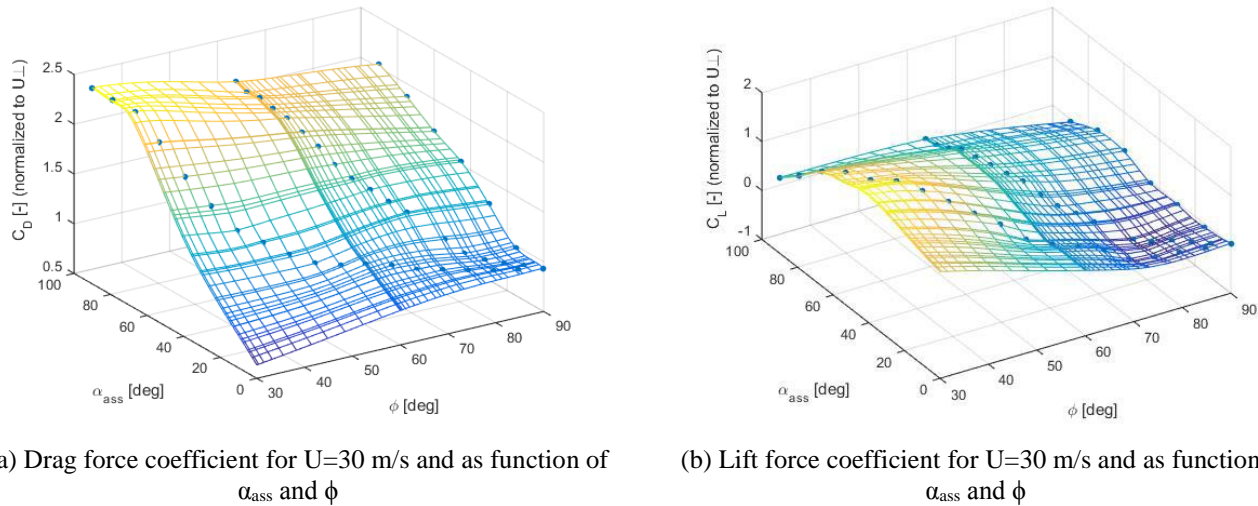(b) Lift force coefficient for U=30 m/s and as function of α_{ass} and ϕ

Figure 10 Force coefficient surface

Using a simplified quasi-steady approach, the condition for the occurrence of galloping can be expressed by the so called Den Hartog criterion.

$$\left(\frac{\partial C_L}{\partial \alpha} + C_D \right)\Bigg|_{\alpha=\hat{\alpha}} < 0$$

Where $K_L = \partial C_L / \partial \alpha$ is the lift derivative with respect to the led orientation angle.

Table 7 summarizes the values of lift derivative and drag for the cable orientations investigated:

β	θ	α_0	$\dfrac{\partial C_L}{\partial \alpha}$	C_D	$\left(\dfrac{\partial C_L}{\partial \alpha} + C_D \right)\Big\|_{\alpha=\hat{\alpha}}$
90	30	0	-0.53	0.94	0.41
90	30	90	-0.50	2.04	1.54
90	60	0	-0.37	0.95	0.58
60	30	0	-0.47	0.87	0.40
30	60	0	-0.43	1.51	1.08

Table 7 Den Hartog criterion for the orientations investigated

In the case of wind perpendicular to the cable ($\beta = 90°$) we have two led orientation angles showing a negative lift derivative: $\alpha_0 = 0°$ and $\alpha_0 = 90°$. In the second case the drag is much higher, resulting in a more critical condition for the first case of $\alpha_0 = 0°$. Also in some other orientation negative lift derivatives have been identified, showing similar slopes.

Basing on the data in Table 7 no instability phenomena are expected according to the Den Hartog criterion. In order to consider simultaneously the effects of other parameter in the galloping instability Macdonald and Larose criterion (2006) for inclined cable was applied. This criterion extended the one developed by Den Hartog introducing the dependence of the stability on other parameters as Reynolds number and all the rotation angles. Also this criterion did not highlight instability problems Nevertheless, according to literature data, these criterions, based on a quasi-steady approach, have limitations in the analysis of the aerodynamic

stability in case of the presence of non-stationary aerodynamic phenomena. This is the case of bluff bodies where often vortex shedding and instability (like galloping) occurs. For this reason further analysis were carried out during dynamic tests.

3.1.3.2   Dynamic tests

Dynamic tests on led configuration were performed in the same way as for roped configuration. Vortex shedding phenomenon was studied for different level of structural non-dimensional damping (see Table 8). The tested values are comparable with the ones relative to roped configuration (see Table 5).

	ζ_s (small amp.)	Sc
	[-]	[-]
r0	1.90E-03	6.6
r1	5.00E-04	1.7
r2	1.00E-04	0.35

Table 8. Structural damping levels

The dynamic behavior of led cable was investigated considering the cable axis perpendicular to the wind (see Table 9).

| θ	β	φ	α	α_0	ζ_s
[deg]	[deg]	[deg]	[deg]	[deg]	[-]
30	90	90.0	0.0	0.0	r0,r1,r2
30	90	90.0	0.0	90.0	r0,r1,r2

Table 9 Dynamic tests on led cable

Significant oscillation amplitudes were registered only for $\alpha_0 = 0°$ while for $\alpha_0 = 90°$ vortex shedding did not occur. In this configuration the gap between the spoke and the cable carrying the led power supply probably destroys the vortices detached by the spoke avoiding vortex induced vibrations.

In Figure 11 are reported the steady state responses of the cable in cross-wind direction for the configuration β=90° - θ=30° - α_0=0°, in particular Figure 11 (a) shows the behavior of the model for different level of structural damping and Figure 7(b) shows the comparison between the two tested cables (roped and led). The dynamic response was obtained exciting the first flexible mode of the model in the cross-wind direction ($f_N = 3.2$ Hz) changing by small step the wind velocity. The data are reported as a function of the velocity ratio calculated as the ratio between current wind velocity and Strouhal velocity ($U_S = f_N D/St = 1.52$ where the Strouhal Number St was evaluated equal to 0.2). It is possible to note that, also for the led cable, a reduction of non-dimensional structural damping increases the maximum amplitude reached in the lock-in region and pushes the synchronization region toward higher velocity ratios. The maximum oscillation amplitudes reached for led cable are higher than the ones obtained in the correspondent roped cable configurations. Moreover the lock-in regions are sensibly wider.

Out of the lock-in region the oscillation amplitudes are quite small and no galloping instability was observed (oscillation amplitudes lower than 2% of the cylinder diameter). This confirms the results obtained applying quasi-steady approach to force coefficients measured on the led cable.

A further confirmation is given by the results of decay tests performed out of the lock-in region: an increase in the aerodynamic non dimensional damping give evidence of the cable stability.
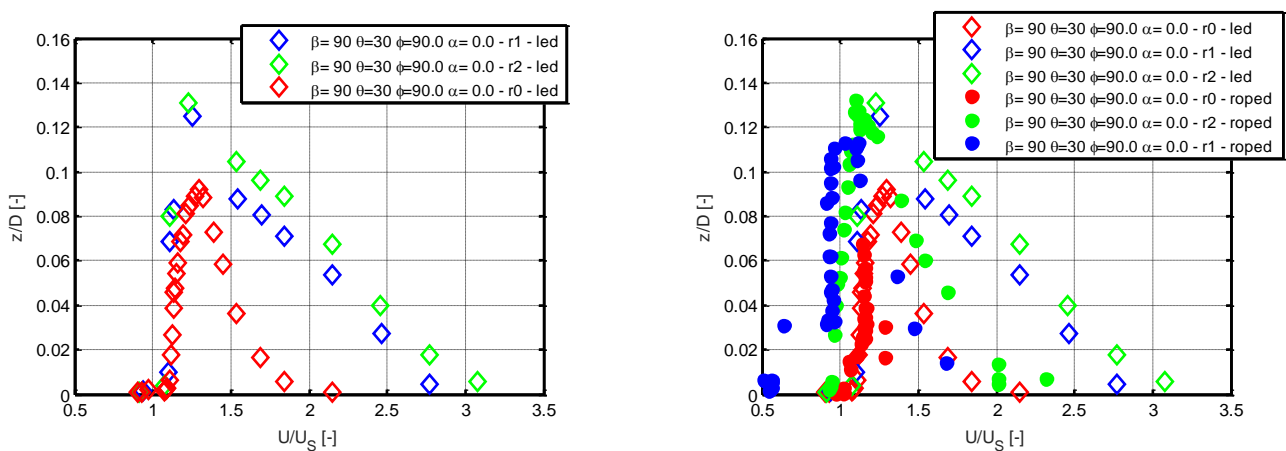
(a) Steady state response for the configuration β=90° e θ=30° for different levels of structural damping

(b) Steady state response for the two types of cable (roped and led) for different values of structural damping

Figure 11 Steady state response

3.2   Supporting structure

The supporting structure is an A-frame, realized with 4 legs arranged as in Figure 12a, the hub height is 137.5m. The leg is a 6.24 meter diameter steel pipe, whose mass per unit length is 7 ton/m. The structural damping is expected to be very low, resulting in a Scruton Number (eq. (1)) lower than 2.

$$Sc = \frac{2\pi m_u \zeta}{\rho D^2}$$

(1)

Due to the leg shape (circular cylinder) and lightness, this structure may be prone to experience flow induced vibrations like vortex induced vibrations, galloping, flutter or wake induced vibrations.

3.2.1   A-Frame wind tunnel model

To investigate these issues we realized an aeroelastic 1:78 scaled wind tunnel model of the A-frame structure (Figure 12b). The model is designed according to the *equivalent model* method. In the equivalent models the physical properties that have to be reproduced are divided in two mechanical parts on the model: an internal structural part that reproduces the stiffness properties and an external skin that reproduces the exterior geometry. The sum of the mass of the internal structure and of the external skin must match the prototype mass scaled. This method is effective for structures in which flexural and torsional effects predominates that is the case of structures such as the A-Frame under investigation. In Figure 12b an aluminum spine reproduces the leg stiffness while the external shield id made by polyurethane tubes. It is to note that the external shield is not continuous for all the tower height but it is divided in shorter parts being each one fixed to the internal spine: this to avoid the external shell to introduce additional stiffness. The model reproduces the first modal shape and natural frequencies of the real structure according to the scaling rules of aeroelastic models.

The wheel is not reproduced in the wind tunnel model. The effect of the wheel mass and stiffness on the mode shapes and frequencies is considered replacing the wheel by a calibrated concentrated mass at brace location: the value of the concentrated mass has been performed by an optimization on a F.E. model and checked on the physical model. Of course the aerodynamic interference between the rim and the A-frame is not reproduced, but the present condition is judged to be conservative with respect to possible flow induced vibrations on the A-frame.

More than one mode shape may be involved in vibrations phenomena and the lower frequencies mode shapes involving the deflections of the legs are the ones to be investigated. The results presented in the paper are related to the first 2 vibration modes in Y direction that are showed in Figure 13.

We give particular attention to the structural damping since this is the main parameter that controls the vibration level. Initially the model structural damping is kept as low as possible in order to better highlight the VIVs. If the tests highlights significant vibrations, the effect of damping is investigated increasing its value up to a reduction of the vibration amplitude below a threshold level. In the present work, a device for a precise damping regulation has been used (Cazzulani et al., 2013, Rocchi et al., 2013). The solution consists in an active control of the damping ratio associated to the vibration modes of the model interested by the wind-structure interaction. The active control, performed through a number of piezoelectric patch actuators bonded to the model itself, allows to independently regulate the damping ratios of the different modes. Eight accelerometers are used to measure the model vibration levels placed at the hub height and at the antinodes of the modes under investigation.

Tests are performed in smooth flow. The wall boundary layer thickness is about 0.2m and the maximum mean velocity deviation across the section outside the boundary layer is less than 3%. The turbulence intensity indexes outside the boundary layer are just below 2%. The average along wind integral length scale is evaluated equal to 0.15m.
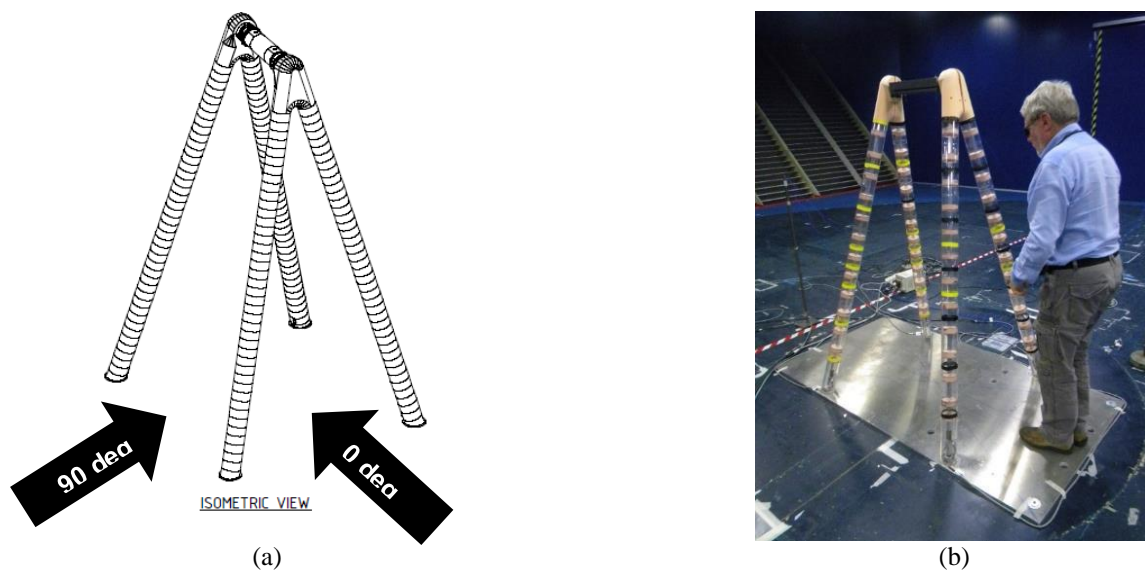

(a)   (b)

Figure 12. (a) Layout of the A-Frame. (b) 1:78 wind tunnel model.

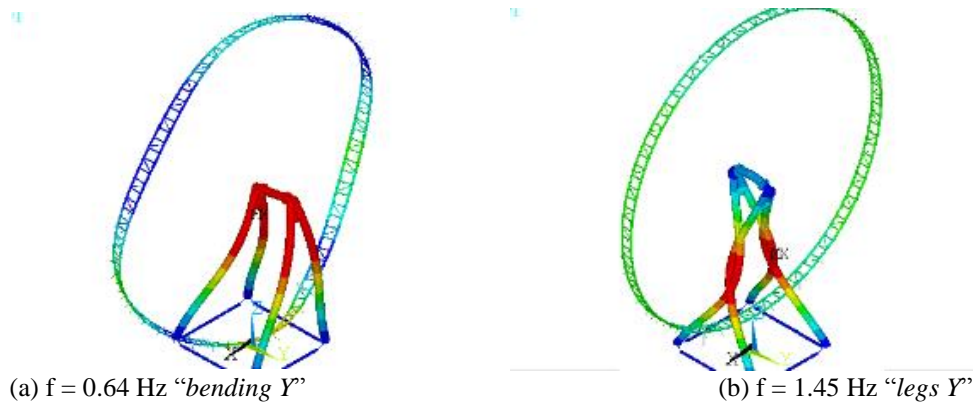(a) f = 0.64 Hz "*bending Y*"   (b) f = 1.45 Hz "*legs Y*"

Figure 13. A-Frame mode shapes that may experience vortex induced vibrations.

3.2.2 Effects of the Reynolds Number on vortex induced vibrations

One important issue in this study is the lack in Reynolds number similitude in the wind tunnel model: according to the definition of Re ($Re = \rho V D / \mu$), if one wants to perform tests on a model having the same Reynolds number of the prototype, the velocity scale factor results as the reciprocal of the geometric scale factor. Tests on a 1/100 scaled model would require a model velocity 100 times higher than the prototype that is in the order of 1000 m/s that is not practicable and will cause distortions due to compressibility effects (compressibility is negligible only for Mach Number < 0.3). The alternative is to perform tests in a different fluid (water) or in a pressurized wind tunnel but these methods are often non feasible. We have to accept that Reynolds similitude cannot be achieved in boundary layer wind tunnel tests. Usually this is not a serious limitation since a Reynolds Number independence is found in many practical situations (bodies with sharp edges). On the contrary, there are particular situations, as when studying structures with curved surfaces like cylinders, where scale effects can be important and must be estimated. Hence the general requirement for large wind tunnels that can host large models and reduce scale effects. An alternative is performing tests at different wind velocities and/or at different model scales to identify possible Reynolds effects on the force coefficients. To improve local flow similarity model curved surfaces are sometimes roughened.

Considering a cylindrical section, the effects of the Reynolds Number is not only on the mean aerodynamic force coefficients ($C_D = C_D(Re)$), but also on the dynamic phenomena as vortex shedding. Figure 14 shows the drag coefficient versus Reynolds Number for a smooth circular cylinder in low turbulence flow where it is possible to identify three regions, named *subcritical* ($Re < 2 - 3 \cdot 10^5$), *critical* (drag coefficient drops) and *postcritical* ($Re > 3 - 6 \cdot 10^6$). As is well known from studies using still cylinders, (Schewe, 1983 ,Zdravkovich, 1997), the Reynolds Number too strongly influences interaction between the cylinder and the incoming flow. In particular, the vortex shedding phenomenon is well defined in the subcritical Reynolds Number range, where it is markedly periodic and the wake has a narrow band spectrum. In the critical region, the phenomenon has reduced magnitude, the harmonic content of the wake covers a wide frequency range and sometimes disappears. Regular vortex shedding can be seriously disrupted if the separation line is not straight (Bearman, 1984), as in the critical region.
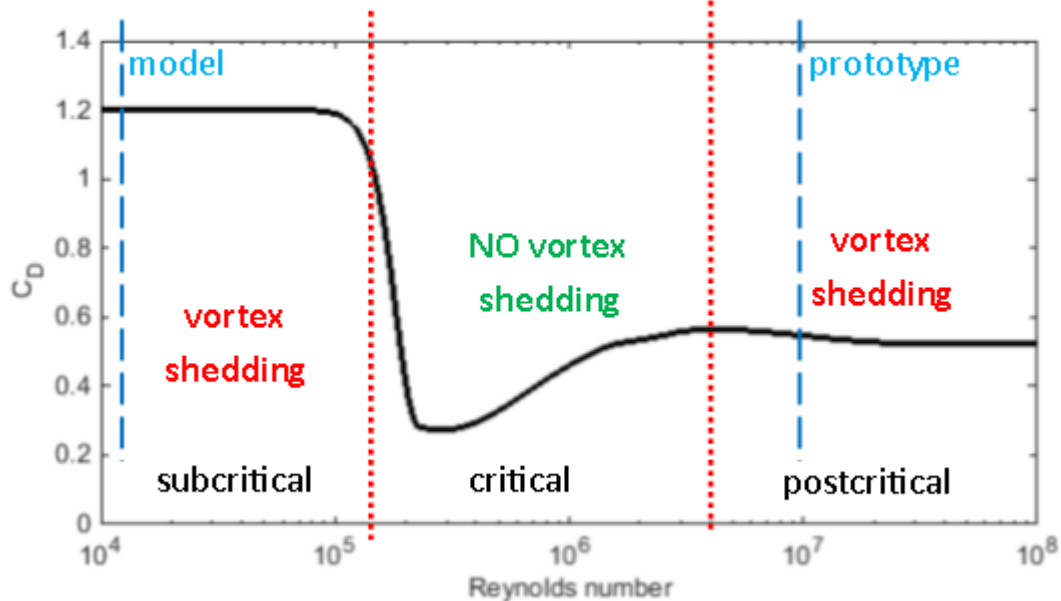

Figure 14. Drag coefficient versus Reynolds Number for a smooth circular cylinder in low turbulence flow.

Nevertheless, recent studies observed vortex induced vibrations in the critical region (Ding et al., 2004, Raghavan and Bernitsas, 2011, Pastò, 2008), but further analysis are necessary to completely define the phenomenon in this condition. (Roshko, 1961) found that vortex shedding reappears at higher Reynolds Numbers, in what is called the postcritical flow regime. In this condition, laminar-turbulent transition occurs within the attached boundary layer and a straight separation line is re-established. Surface roughness affects vortex shedding owing to its effects on the body's surface characteristics and consequently on the boundary layer (Buresti, 1981).

Many studies (Buresti, 1981, Zdravkovich, 1997) reported that the presence of roughness on the cylinder's surface anticipates the laminar-turbulent transition in the boundary layer and also the 'drag crisis region' at smaller Reynolds Numbers.

Considering the A-Frame cylindrical legs diameter, the real structure is operating at very high Reynolds number ($Re \approx 10^7$, that is a postcritical flow regime). As previously stated, it is not possible to perform tests on the model at the same Re. According to the scale factors the model Reynolds Number is in the order of $Re \approx 10^4$

This problem can be overcome considering that the vortex shedding mechanism in the supercritical region is similar to that in the subcritical region (Belloli et al., 2007, 2015; Diana et al., 2007, 2008; Zasso et al., 2008). We give here a summary of the results of these studies. Figure 15 compares the non-dimensional oscillating amplitudes, A/D, of a rigid circular cylinder in the Williamson and Roshko's map of the vortex (Williamson and Roshko, 1988). The figure shows data obtained at low Reynolds Numbers (subcritical and lower) compared to tests at postcritical Reynolds Numbers. Comparing the experimental result in subcritical and postcritical conditions at similar Scruton number, Even if some differences can be observed, the lock-in behavior is significantly similar in the two cases (Belloli et al., 2015). In particular, the specific power input curve as function of the non dimensional vibration amplitude comparison (Figure 16) shows a very good agreement, this latter fact is very important under a practical point of view, because the numerical models used at low Reynolds could be adopted also in postcritical flow conditions.

On these bases, the tests on the A-Frame scaled model are performed in subcritical flow regime in smooth flow conditions: this situation is assumed to be conservative with respect to flow induced vibrations excitation mechanism.
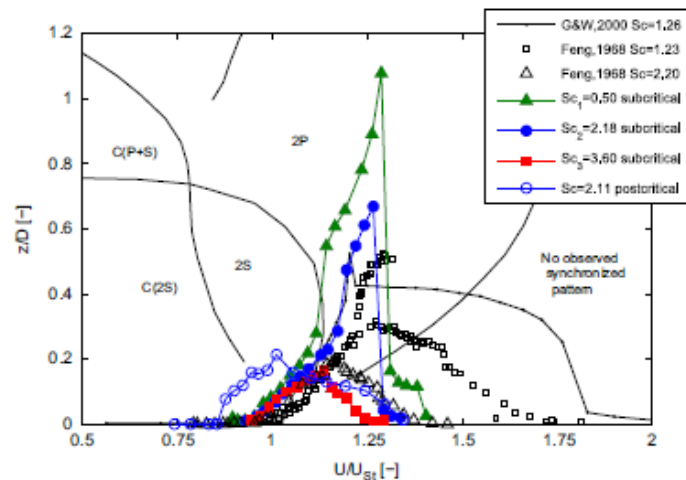

Figure 15 Free vibration cylinder response in the plane A/D vs. U/USt. Zasso progressive regimes (Zasso et al., 2006) data have been compared with Feng results (Feng, 1968) and Govardhan&Williamson results (m*=320 , m*ζ=0.256 , Re=1250) (Govardhan and Williamson, 2000).
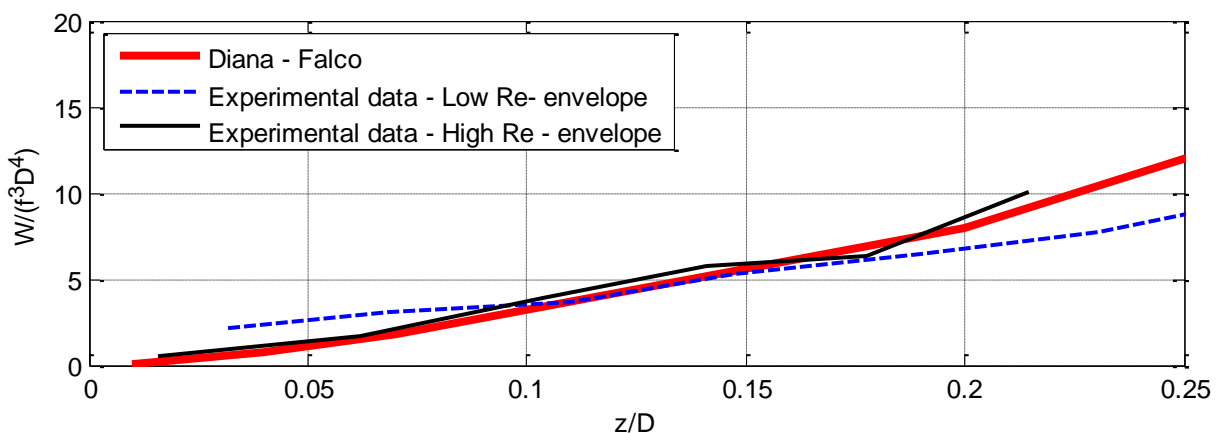

Figure 16 Power input on a rigid cylinder: comparison between the experimental data envelope curve obtained at high (postcritical) and at low (subcritical) *Re* conditions and the literature reference data (Diana, 2007)

3.2.3   A-Frame flow induced vibrations results

The tests showed the presence of vortex induced vibrations that, in case of very low structural damping, can reach high amplitudes that the structure cannot tolerate. No other aeroelastic instabilities have been identified on the A-frame model (e.g. galloping, flutter, wake induced vibrations. Figure 17 shows the model displacement as a function of the test wind velocity, having the wind blowing at 90 degrees according to Figure 12a. It is possible to observe two lock-in regions where the A-Frame experiences cross wind vibrations due to vortex shedding. The first peak is observed at 1.9 m/s while the model is vibrating according to mode 1 (Figure 13a): maximum displacement is measured at hub height and the corresponding Strouhal number is 0.17. The second lock-in region is at 7.0 m/s according to mode 5 and the maximum displacement is measured about at half leg length (Figure 13b), having also the same Strouhal.

As previously discussed, in order to control the vibration level the structural damping must be increased. Wind tunnel tests are able to define the relationship between the structural damping and the vibration amplitude. Different damping levels have been investigated for both the lock-in regions. Figure 18a shows the A-frame response for mode 1 as a function of the wind velocity: data are reduced to full scale values: peak response is measured for a wind speed equal to 23.6 m/s and, as expected, reduce its magnitude increasing the damping to critical damping ratio. This relationship is usually presented having the displacement as a function of the damping as in Figure 18b where it is visible how the amplitude reduces with damping. The same analysis is showed in Figure 19 for the second analyzed mode: in this case the critical wind velocity is quite high (55 m/s) that unlikely will be experienced by the structure during its lifetime.

In order to compare the experimental result with the literature ones on circular cylinders (EPRI 2006), the results of Figure 18b and Figure 19b are presented in Figure 20 where the oscillation amplitudes are normalized to the leg diameter and the damping is expressed in terms of Scruton number. Results of mode 1 are below the reference data: this probably because in the A-Frame structure there is some aerodynamic interference between the legs and hub so that vortex shedding force is reduced with respect to the expected amplitudes on an isolated, infinite length, circular cylinder. On the contrary, results of the second mode are slightly higher. It is to point out that the reference curve refers to an isolated cylinder while in ta A-frame there are four cylindrical legs with different inclination angles and possible shielding effects.

In order to control the vibration level on the real structure, mitigation devices have to be taken into account in order to increase the structural damping.
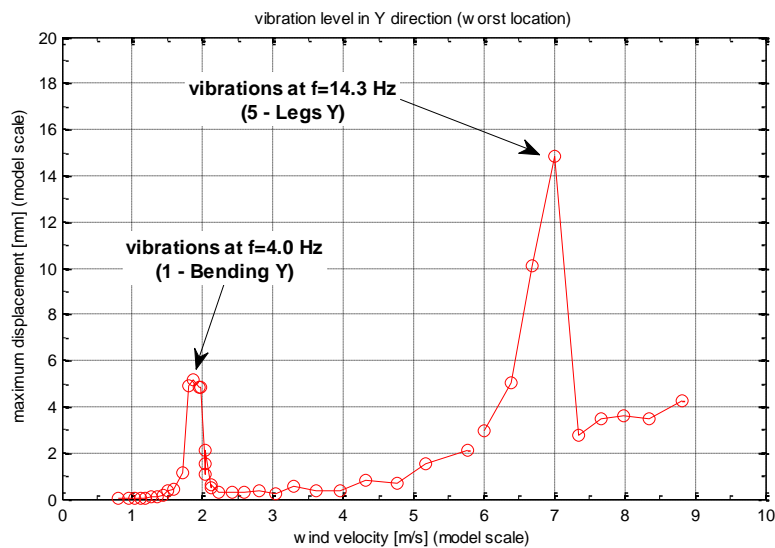

Figure 17. Model vibration frequencies as a function of the wind velocity: Y direction,
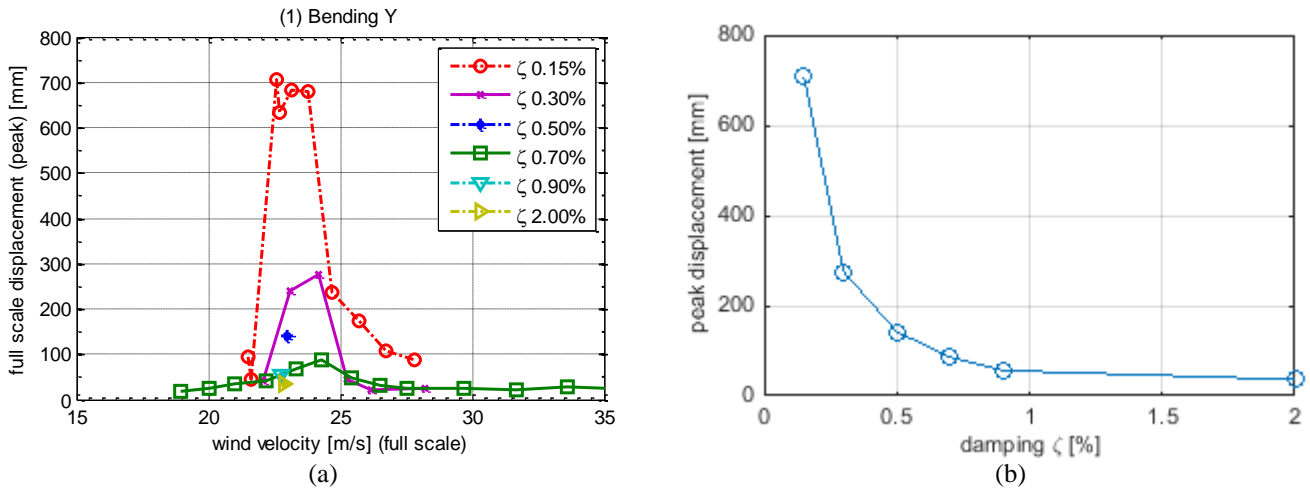exposure 90 deg, low damping

(a)

(b)

Figure 18 Vibration mode 1: full scale peak displacement as a function of the wind velocity for different structural damping levels (a) and peak displacement as a function of the structural damping level (b)
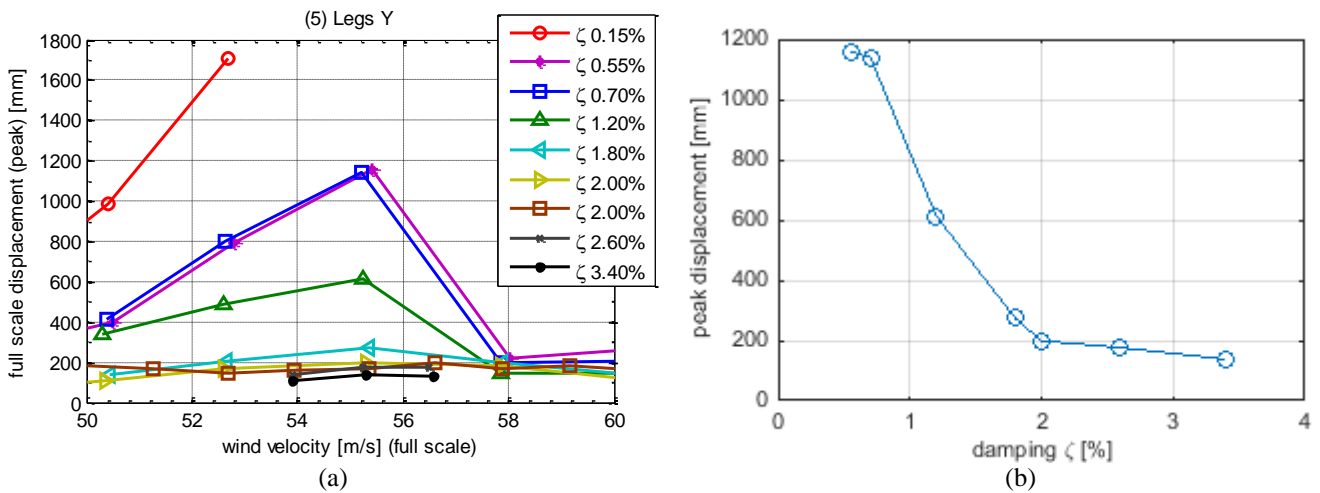

(a)

(b)

Figure 19 Vibration mode 5: full scale peak displacement as a function of the wind velocity for different structural damping levels (a) and peak displacement as a function of the structural damping level (b)
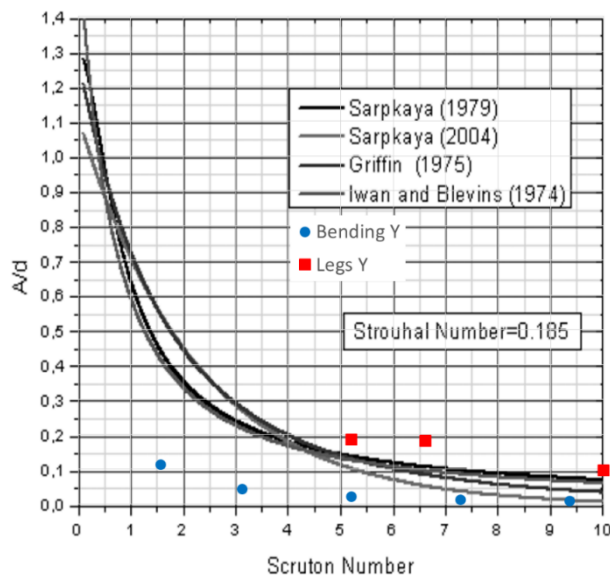

Figure 20. Maximum vibration amplitude as a function of the Scruton number.

3.2.4   Mitigation devices

One of the most used devices to control vibrations are the Tuned Mass Dampers (TMDs). The main purpose of the TMD is to increase the structure damping up to the value for which the vibration amplitudes are controlled within prescribed value. It is a normal practice in VIV to adopt as limit value for the vibrations, the maximum acceleration. As an example, in case of tall buildings, for people comfort the maximum acceleration value is taken as 0.2 m/s^2. In case of the towers of structures like bridges, the limit is generally taken around $1 \div 2$ m/s^2. The TMD mass should be of the range of 1/100 of the modal mass of the mode to be controlled, in order to have a damping increment in the order of 2%. The modal mass should be referred to the maximum amplitude of the considered mode and the TMD should be possibly placed where the maximum amplitudes occur. Basing on these considerations the mass of the TMD can consist of several tons (25-90), depending on the mode under investigation and the target damping level.

For an accurate design of the TMD, a suitable numerical approach has been used to reproduce the A-frame response to vortex excitation. This numerical approach can also reproduce the response to vortex shedding of the A-frame equipped with TMDs, allowing for the optimization of the TMD parameters in order to control vibrations below an acceptable value (defined for this case study as 0.05m) that, without TMD, would be of the order of 1 m. On the basis of modal analysis from the FE model of the structure and on the WT results, an equivalent oscillator model is tuned according to reproduce the VIV (Diana and Gasparetto, 1980; Manenti et al. 2007).

The equivalent oscillator model is an additional system that can introduce energy into the structure, reproducing the lock-in phenomenon energy input and synchronization effect. The TMD is connected to the structure that has its own stiffness, and which in turn is excited by the equivalent oscillator effect (see Figure 21 sketch). The analysis is carried out in the time-domain, so as to take into account the non-linearity related to the equivalent oscillator. There are several parameters of the equivalent oscillator that need to be tuned in order to match the experimental results. Once the parameter of the model are properly tuned, the equivalent oscillator model can reproduce the amplitude of vibration in the "lock-in" region, also for different structural damping ratio supposed for the structure.
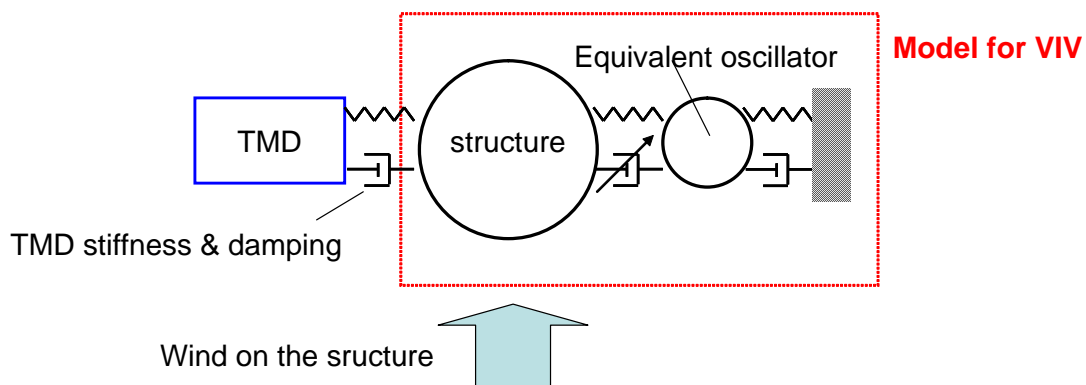

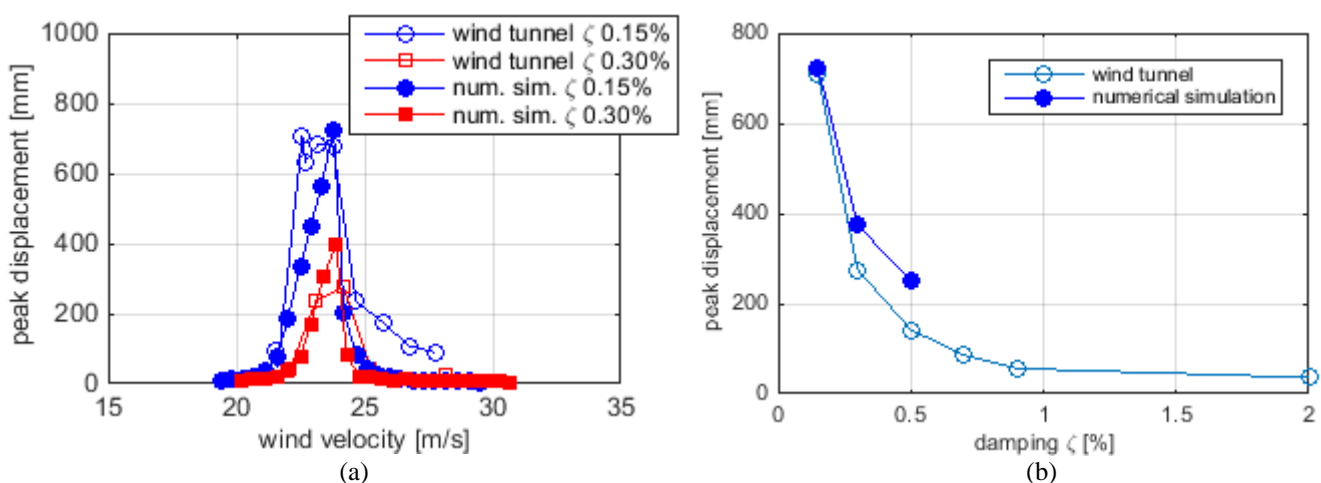Figure 21 Principle of the VIV model applied on the structure, and the addition of the TMD.

(a)

(b)

Figure 22 *Bending Y* mode: comparison between wind tunnel test results and simulation, for 0.15% and 0.3% structural damping

(a) wind time history

(b) structure response at hub location without TMD

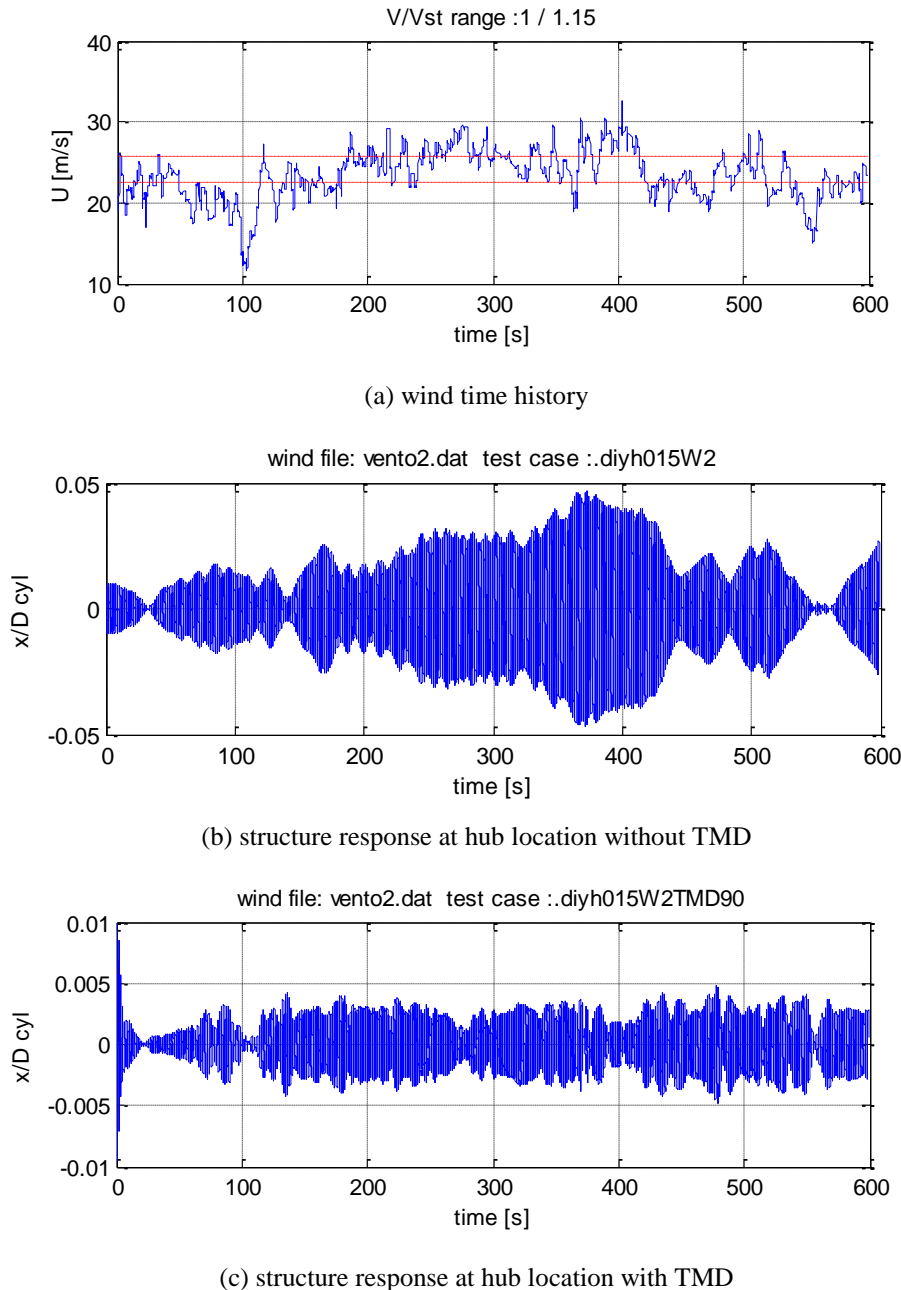(c) structure response at hub location with TMD

Figure 23 Structure response in lock-in and turbulent wind condition

Figure 22 shows progressive regimes results of the wind tunnel tests compared with the equivalent oscillator model numerical simulation results for mode 1 and two different structural damping levels: it is possible to observe that a correctly tuned oscillator can reproduce the lock in phenomenon with an high accuracy level.

Then 3 different scenarios are considered for the operation of the TMDs:
- lock-in condition in smooth flow
- lock-in condition in turbulent flow
- buffeting response to high winds (out of lock-in)

The simulation showed that under smooth wind a set of perfectly tuned TMDs with a total mass of 80 tons can suppress the VIV.

Then, in order to identify the TMD behavior in transient conditions, simulations in turbulent wind and lock in are achieved. Figure 23a shows the numerical wind time history used for the simulations: the wind ranges in V/V_{St} 1 ÷ 1.15 and the subsequent figures Figure 23b and c shows the normalized structure displacement without and with dampers. We can observe that also in transient conditions the vibration level is significantly reduced by the dampers (about 10 times).

Finally Figure 24 shows the buffeting response under strong winds (40 m/s): we observe how the TMDs can also control the amplitudes of vibration for the maximum wind speed, that is outside the lock-in region (Diana et al., 1979).
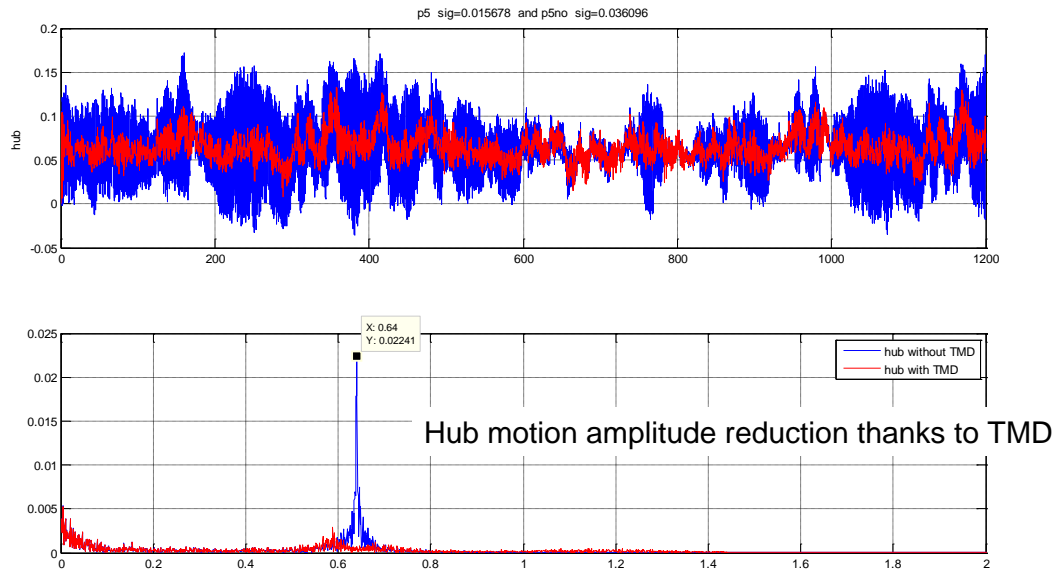
Figure 24 Hub motion with the maximum turbulent wind. Withou TNMD (blue line), with TMD perfectly tuned (red line). mean speed 40m/s, It=12%. 2x40=80 tons and h=10%

4   CONCLUSIONS

The paper reviewed the aerodynamic design of big observation wheels highlighting the possible sources of wind induced vibrations like vortex shedding, galloping and wake induced vibrations. A case study is presented showing the investigation of these phenomena by means of wind tunnel tests and numerical models.

The main issue are vortex induced vibrations that can affect several components of the structure: spoke cables and A-frame. In case of light and low damped structures vibration amplitudes can reach significant amplitudes. Wind tunnel tests are often used to support the wheel design.

Aim of the tests is to define the requirements for the design of mitigation devices like hydraulic or tuned mass dampers.

5   ACKNOLEDGEMENTS

6   REFERENCES

Allsop, A., Dallard, P. & McNiven, B. 2009, The Singapore Flyer and design of giant observation wheels, Singapore, Structural Engineering International: Journal of the International Association for Bridge and Structural Engineering (IABSE), vol. 19, no. 1, pp. 12-16.

Bearman, P.W., 1984. Vortex shedding from oscillating bluff bodies. Annu. Rev. Fluid Mech. 16,195–222.

Belloli, M., Giappino, S., Muggiasca, S. & Zasso, A. 2007, Vortex shedding on circular cylinder at critical and postcritical Reynolds Number, Seventh International Symposium on Cable Dynamics, December, 10-13.

Belloli, M., Giappino, S., Morganti, S., Muggiasca, S. and Zasso, A., 2015, Vortex induced vibrations at high Reynolds numbers on circular cylinders, Ocean Engineering, Volume 94, Pages 140-154, ISSN 0029-8018, http://dx.doi.org/10.1016/j.oceaneng.2014.11.017.

Buresti, G., 1981. The effect of surface roughness on the flow regime around circular cylinders. J. Wind Eng. Ind. Aerodyn. 8, 105–114.

Carassale L., Freda A., Piccardo G., 2005. Aeroelastic forces on yawed circular cylinders: quasi-steady modeling and aerodynamic instability. Wind and Structures, Vol. 8, No. 5 (2005) 373-388.

Cazzulani, G., Balduzzi, T., Ripamonti, F., Rocchi, 2013. D. Active damping for wind-tunnel aeroelastic models of large civil structures (2013) Proceedings of SPIE - The International Society for Optical Engineering, 8690, art. no. 869003.

Chen, S., 1987, Flow-induced vibration of circular cylindrical structures, Hemisphere Pub. Corp., Washington.

Cheng, S., Larose, G.L., Savage, M.G., Tanaka, H. & Irwin, P.A. 2008, Experimental study on the wind-induced vibration of a dry inclined cable-Part I: Phenomena, Journal of Wind Engineering and Industrial Aerodynamics, vol. 96, no. 12, pp. 2231-2253.

Cigada, A., Manenti, A. & Vanali, M. 2000, Wind action on the London eye cables. Part II: damping device design and field measurements, Invento, Genova, Italy.

Den Hartog, J.P., 1932. Transmission Line Vibration Due to Sleet. Transaction, AIEE, 1074-1076.

Diana, G. & Falco, M., 1971. On the forces transmitted to a vibrating cylinder by a blowing fluid. Meccanica, N. 1 Vol. 11 pp 1-17.

Diana, G., Di Giacomo, G., Claren, R., 1979. An approach to vortex shedding under turbulence air flow on a single vibrating cylinder, IEEE paper A 79 529-9

Diana, G., Gasparetto, M., 1980. "Simulation of vortex shedding by means an equivalent oscillator". L'Energia elettrica.

Diana, G., Cheli, F., Resta, F., Zasso, A. & Marini, M., 2000, Wind action on the London eye cables. Part I: modelling of the cables dynamic response, Invento, Genova, Italy.

Diana G., Cigada A., Belloli M., Rocchi D., 2003. Wind tunnel investigation on vortex induced vibration of a long flexible cylinder 5th International Symposium on Cable Dynamics, Santa Margherita Ligure, Italy.

Diana, G., Belloli, M., Giappino, S., Muggiasca, S. & Zasso, A. 2007, The effect of Reynolds Number on aeolian vibrations, Seventh International Symposium on Cable Dynamics, December, 10-13.

Diana, G., Belloli, M., Giappino, S. & Muggiasca, S. 2008, Vortex induced vibrations at high Reynolds Numbers, VI International Colloquium on Bluff Bodies Aerodynamics & Applications BBAA VI, July, 20-24.

Ding, J., Balasubramanian, S., Lokken, R., Yung, T., 2004. Lift and damping characteristics of bare and staked cylinders at riser scale Reynolds numbers, Proceedings of the Annual Offshore Technology Conference, vol 1. Offshore Technology Conference, Houston, TX; United States, pp. 518–526, ISBN 01603663.

EPRI Transmission Line Reference Book: Wind-Induced Conductor Motion. EPRI, Paolo Alto, CA: 2006. 1012317

Hartlen R. T. and Currie I. G., Lift-oscillator model of vortex vibration. Journal of Engineering Mechanics, vol. 96, pp. 577-591, 1970.

Hogan J.D., Hall J.W., 2010. The Spanwise Dependence of Vortex-Shedding From Yawed Circular Cylinders. Journal of Pressure Vessel Technology JUNE 2010, Vol. 132 / 031301-5

Jain A.B., 2012. Vortex-Induced Vibrations of an Inclined Cylinder in Flow. Masters Theses 1896 - February 2014. Paper 911

Jakobsen, J.B., Andersen, T.L., Macdonald, J.H.G., Nikitas, N., Larose, G.L., Savage, M.G. & McAuliffe, B.R. 2012, Wind-induced response and excitation characteristics of an inclined cable model in the critical Reynolds number range, Journal of Wind Engineering and Industrial Aerodynamics, vol. 110, pp. 100-112.

Luongo A., Piccardo G., 2005. Linear Instability for Coupled Translational Galloping. Journal of Sound and Vibration, 288(4-5), 1027-1047

Macdonald, J.H.G. & Larose, G.L. 2006, A unified approach to aerodynamic damping and drag/lift instabilities, and its application to dry inclined cable galloping, Journal of Fluids and Structures, vol. 22, no. 2, pp. 229-252.

Manenti A., Resta F., Belloli, M. and Muggiasca, S. & Zasso, A. 2007. Aeolian Vibrations of Overhead Transmission Lines: A Comparison Among Time and Frequency Domain. Seventh International Symposium on Cable Dynamics, December, 10-13.

Matsumoto M., 1998. Observed Behaviour of Prototype Cable Vibration and its Generation Mechanism. Bridge Aerodynamics, Larsen & Esdahl (eds), Balkema, Rotterdam, 189-211.

Matsumoto, M., Yagi, T., Shigemura, Y. & Tsushima, D. 2001. Vortex-induced cable vibration of cable-stayed bridges at high reduced wind velocity. Journal of Wind Engineering and Industrial Aerodynamics, vol. 89, no. 7-8, pp. 633-647.

Matsumoto M., Yagi T., Hatsuda H., Shima T., Tanaka M., Naito H., 2010. Dry galloping characteristics and its mechanism of inclined/yawed cables. Journal of Wind Engineering and Industrial Aerodynamics 98(2010), 317–327

Observation Wheel directory, Guide to the World's Largest Ferris wheels. www.observationwheeldirectory.com

Pastò, S., 2008. Vortex-induced vibrations of a circular cylinder in laminar and turbulent flows. J. Fluids Struct 24, 977–993.

Raghavan, K., Bernitsas, M. M., 2011. Experimental investigation of Reynolds number effect on vortex induced vibration of rigid circular cylinder on elastic supports. Ocean Eng. 38, 719–731.

Rocchi, D., Balduzzi, T., Cazzulani, G., Argentini, T, 2013. Active damping devices for aeroelastic models (2013) 6th European and African Conference on Wind Engineering, EACWE 2013.

Roshko, A., 1961. Experiments on the flow past a circular cylinder at very high Reynolds number. J. Fluid Mech. 10, 345–356.

Schewe,G.,1983.On the force fluctuations acting on a circular cylinder in crossflow from subcritical up to transcritical Reynolds numbers. J.FluidMech.133, 265–285.

Williamson, C. H. K., Roshko, A., 1988. Vortex formation in the wake of an oscillating cylinder. J. Fluids Struct 2, 355–381.

Zasso, A., Belloli, M., Giappino, S. & Muggiasca, S. 2008, Pressure field analysis on oscillating circular cylinder, Journal of Fluids and Structures, vol. 24, no. 5, pp. 628-650.

Zdravkovich, M. M., 1997. (Foundamentals). Flow Around Circular Cylinders, 1. Oxford University Press, Oxford, New York.

Zhao F., Ding J., 2010. Nonlinear Analysis and Research of Flexible Giant Ferris Wheel. IEEE 978-1-4577-0290.